CLOUD FORCING: A MODELING PERSPECTIVE

Gerald L. Potter,[1] Julia M. Slingo,[2] Jean-Jacques Morcrette[3]
Robert L. Mobely[1], Robert S. Drach[1], Thomas G. Corsetti[1] Dean N. Williams[1]

[1]PCMDI, Lawrence Livermore National Laboratory, Livermore, Caifornia, U.S.A.
[2]Department of Meteorology, University of Reading, Reading, Berkshire, U.K.
[3]European Centre for Medium-range Weather Forecasts, Reading, Berkshire, U.K.

ABSTRACT

Radiation fields from a perpetual July integration of a T106 version of the ECMWF operational model are used as surrogate observations of the radiation budget at the top of the atmosphere to illustrate various difficulties that modellers might face when trying to reconcile cloud radiation forcings derived from satellite observations with model-generated ones. Differences between the so-called Methods I and II of Cess and Potter (1987) and a variant Method III are addressed. Method I is shown to be the least robust of all methods, due to potential uncertainties related to persistent cloudiness, length of the period over which clear-sky conditions are looked for, biases in retrieved clear-sky quantities due to an insufficient sampling of the diurnal cycle.

We advocate the use of Method II as the only unambiguous one to produce consistent radiative diagnostics for intercomparing model results. Impact of the three methods on the derived sensitivities and cloud feedbacks following an imposed change in sea surface temperature (used as a surrogate climate change) is discussed.

1. INTRODUCTION

The concept of cloud forcing was first introduced by Coakley and Baldwin (1984) and later used by Ramanathan (1987) to identify the impact of clouds on the radiation budget at the top of the atmosphere. It may be defined as the difference between the radiative flux which actually occurs with cloudiness and that which would occur if clouds were removed *but the atmospheric state was unchanged.* The change in cloud forcing that accompanies a change in climate is known as the cloud feedback. In a recent study by Cess et al. (1989) of the response of 14 atmospheric general circulation models (GCMs) to an imposed change in sea surface temperature (used as a surrogate climate change), an almost threefold variation in the cloud feedback from

weakly negative to strongly positive was obtained. This led Cess et al. to conclude that cloud-climate feedback could be a significant cause of inter-model differences in climate change projections. While this variation in feedback can be attributed to the difference in the treatment of clouds between the various models, a contributory factor may also be the definition and method of computation of the cloud forcing itself.

Cloud forcing (CF) is defined as:

$$CF = F_{clear} - F_{total} + Q_{total} - Q_{clear} \quad (1)$$

where F and Q are, respectively, the emitted infrared and net downward solar fluxes at the top of the atmosphere. The concept of cloud forcing was originally introduced with satellite data because it allowed the impact of clouds on the top of the atmosphere radiation budget and therefore on the earth/atmosphere system to be determined without requiring any knowledge of the cloud fraction or cloud height, both of which are difficult to measure. Similarly the modeling community has adopted cloud forcing because it circumvents the problems of intercomparing or validating cloud amount and cloud radiative properties, both of which are highly model dependent.

The primary uncertainty in the calculation of cloud forcing lies in the determination of the clear sky fluxes. The original estimates of cloud forcing were computed from satellite data in which the clear sky flux could only be obtained from cloud free pixels. The basic assumption was made that over a reasonable length of time, say one month, the majority of pixels would experience clear skies and thus allow measurement of the clear sky flux. However, while, at the moment, this appears to be the only practical way for estimating the clear sky flux from satellite data, it has the disadvantage that the clear and cloudy fluxes *do not apply to the same atmospheric state*. Additionally, it is conceivable that there may be areas of the globe where the satellite is unable to find any clear pixels and thus unable to estimate the cloud forcing.

Cess and Potter (1987) identified this calculation of the clear sky flux as Method I. For models, an alternative procedure exists in which the clear sky flux is computed whatever the cloudiness. This flux is often already available from the radiation code or can be easily computed by running the code again with clear skies. This method of calculating the cloud forcing was defined as Method II by Cess and Potter. More recently, a hybrid version, intermediate between Methods I and II, has been used in some models. Referred to in this paper as Method III, it weights the clear sky flux, computed as in Method II, by the clear sky fraction.

Radiation budget data from models can be used to calculate the cloud forcing using any of the above methods, since the clear sky flux can be computed from the model's temperature and humidity profiles. Method I has tended to be favored because it allows comparison with the observed cloud forcing from satellite data. However, the adoption of Method I by modellers is fraught with problems. It is not difficult to envisage, thought some simple thought experiments, that the probability of detecting clear skies at any model grid pint may be dependent on the horizontal resolution, the type of cloud prediction scheme used in the model and the presence or absence of a diurnal cycle in the model.

In this paper, radiation fields at the top of the atmosphere (TOA) from a series of integrations of the ECMWF general circulation model run at two different horizontal resolutions are used as surrogate satellite observations to address the validity of the methods of retrieving the clear sky flux, particularly for the purpose of model intercomparison and for the estimation of the cloud feedback in studies of climate change. The methodology and the various methods of retrieving the clear-sky fluxes are described in section 2. In section 3, we review the various uncertainties inherent to Method I. Methods II and III results are then shown in sections 4 and 5, respectively. In section 6, we discuss how the differences in clear-sky fluxes obtained by the various methods influence the sensitivity of the model to an imposed change in sea surface temperature.

2. METHODOLOGY-DESCRIPTION OF METHODS I,II,III

2.1. The model

A general description of the ECMWF forecasting system is given in Hollingsworth et al. (1985), whereas a more detailed discussion of either the dynamical or the parameterization aspects of the model can be found in Simmons et al. (1988) and Tiedtke et al. (1988).

In the ECMWF model, the prognostic variables are represented in the horizontal by truncated series of spherical harmonics. The model uses a triangular truncation, and a T106 horizontal resolution therefore refers to the representation retaining the first 106 spectral coefficients. Physical tendencies are calculated by the physical processes parameterizations on a Gaussian collocation grid where the mesh size is $(1.125^{o})^2$ at T106 and $(5.625^{o})^2$ at T21. All results presented hereafter were obtained with the ECMWF model running at PCMDI (cycle 33 of the libraries, operational in July 1989).

In particular, the model includes the new mass-flux scheme for dealing with convective processes (Tiedtke, 1989) and the new radiation scheme (Morcrette, 1990). Cloud fields are diagnosed with the original cloud scheme of Slingo (1987). The model includes the diurnal cycle of insolation. Full radiation computations are performed every 3 hours and the radiation fields are updated at every time step (Δt = 900 s at T106, Δt = 2700 s at T21) taking into account the proper solar zenith angle in the shortwave and the proper temperature profile in the longwave computations. The model was integrated for surface temperature (SST) of Alexander and Mobley (1976) in the control case, or ± 2K SST perturbations to that climatology in the perturbed cases (SST – 2K, or SST + 2K). In all integrations, instantaneous total and clear-sky radiation fields have been saved every 3 hours. Most results presented hereafter are means over the last 30 days of the integrations and therefore include 240 instantaneous fields.

2.2. Clear sky flux retrievals

In Method I, the clear-sky flux for any model grid point is obtained from:

$$F_{cs} = \frac{\sum_{i=1}^{N} F_i \delta_i}{\sum_{i=1}^{N} \delta_i} \qquad (2)$$

where N is the total number of observations (here the total number of radiation time-steps) and δ_i is 1 if the grid is totally clear-sky and 0 otherwise. F_i is the total flux so that only the fluxes for clear sky conditions are summed in this case. This method can be used with satellite observations provided that information on the state of the atmosphere (clear sky or cloudy) is available. This method gives areas with missing clear-sky "observations" wherever there is always some fractional cloudiness (even not overcast) at the pixel resolution when dealing with actual satellite observations or at the resolution of the model grid when dealing with model fluxes. Such a method is also likely to lead to a different sampling for longwave and shortwave fluxes.

Method II presupposes the availability of clear sky flux at any point and any time. The clear sky flux in a given grid box is given by

$$F_{cs} = \frac{1}{N} \sum_{i=1}^{N} F_i^{clear} \qquad (3)$$

where F_i^{clear} is the clear-sky flux computed by the model.

This method can always be applied in model calculations of the cloud radiative forcings and is a foolproof method for intercomparing model results as the clear-sky flux is always defined whatever the conditions. In practice, depending on the actual details of the radiation code, this method may require running the radiation code twice, once for computing the diagnostic clear-sky fluxes and once for calculating the total fluxes and radiative heating rates to enter the thermodynamic equation of the model.

Method III is somewhat intermediate between Methods I and II. In the context of model simulations, the clear-sky flux is obtained as:

$$F_{cs} = \frac{\sum_{i=1}^{N} F_i^{clear}(1-C_i)}{\sum_{i=1}^{N} (1-C_i)} \qquad (4)$$

where C_i is the total cloudiness over the grid-box at time-step 1, and F_i^{clear} is the clear-sky flux computed by the model. This method has often been adopted as a variant of Method I by modellers whose cloud scheme allows for partial cloudiness. In the case of an "on/off" cloud scheme (cloud cover is either 0 or 1), Method III is equivalent to Method I.

Again this method assumes knowledge of the clear sky flux at every grid point for every time sample, as in Method II. However, unlike Method II, it will be prone to sampling problems because the cloud forcing will not be defined for overcast conditions.

In fact, none of these three methods is really consistent with the elaborate data processing actually carried out on ERBE measurements. As detailed in Harrison et al. (1988), once the radiance measurement has been converted to a TOA longwave flux and a scene identification giving the most probably cloud cover over the observed scene (in terms of clear (0-5%), partly cloudy (5-50%), mostly cloudy (50-95%), and overcast (95-100%), this flux is assigned to one of the 24 local hours in one of the 10,368 regions (2.5° latitude x 2.5° longitude). Even with a multi-satellite ERBE data set (usually two satellites have been contributing), measurements can provide only a

few estimates of the TOA flux during each day for a given region. A complete monthly set of hourly TOA flux for each region is generally determined from linear interpolation between all measured flux values (Brooks et al., 1986). However, over land regions, which have a significant diurnal variation in surface temperature (e.g., deserts), a trigonometric model replaces the linear interpolation. Therefore, both the clear-sky and total ERBE fluxes that have recently been used for deriving cloud forcings (Ramanathan et al., 1989) account for the diurnal cycle. The following sections show that the model results (if they have not been obtained with Method II, which in any case differs from the data processing performed on the ERBE measurements) are very likely not to account properly for the diurnal cycle.

3. METHOD I

3.1. Missing data

As already described, the cloud forcing calculated using Method I is dependent on the number of samples for which the sky is clear during the time period in question. Figure 1(a) shows the percentage incidence of clear skies for the mean of days 61 to 90 from the T106 model. The corresponding cloud amounts are shown in Figure 1(b). The white areas in Figure 1(a) represent missing data, i.e., those grid points for which there were no cloud free days. These occur primarily over the convectively active areas of the tropics and over the region of persistent stratus clouds associated with the cold waters of the North Pacific. The area of missing data over the Himalayas is primarily due to the model's tendency for the monsoon flow over India to track northwards, releasing its precipitation over this region rather than over India itself.

It is clear from Figures 1(a) and 1(b) that the main areas of missing data are coincident with the areas of maximum cloudiness, precisely where the cloud forcing will be large. Similarly, Figure 1(a) also shows that the percentage incidence of clear skies is low over most regions of the globe with good correlation between large amounts of cloud and low percentages of incidence of clear skies, i.e., where the cloud forcing is likely to be large, method I will rely on a small number of samples. ```Thus, both in terms of missing data and of sample size, the cloud forcing is likely to be poorly represented by Method I precisely in those regions where it is important.

The areas of missing data in this 30-day mean from the ECMWF model run at T106 horizontal resolution are quite extensive and probably arise from the model's tendency to produce a very persistent location for the ITCZ, which is more marked at

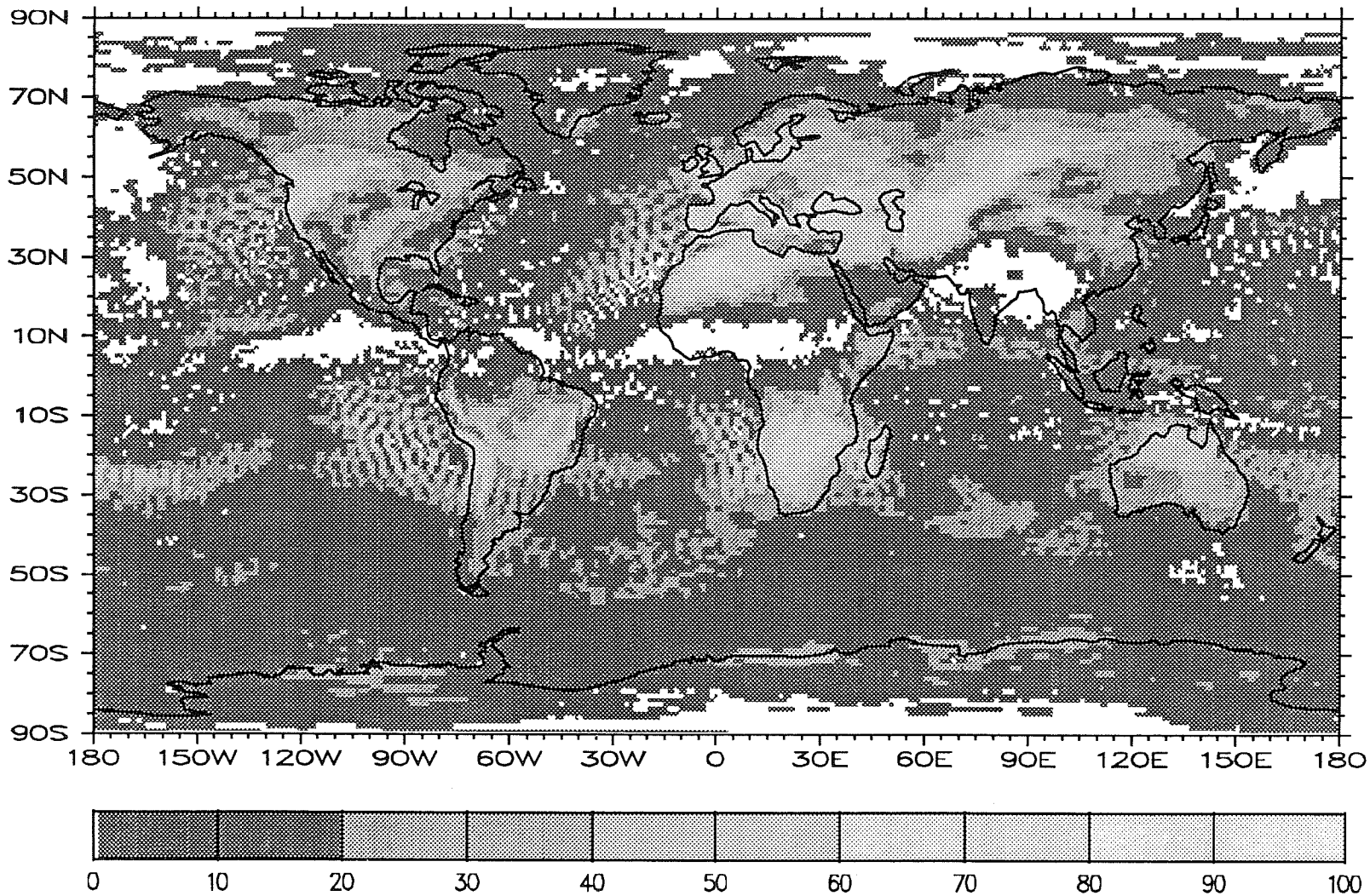

Figure 1a: The incidence of clear-sky observations in percent during the last 30 days of a T106 90-day perpetual July integration (%).

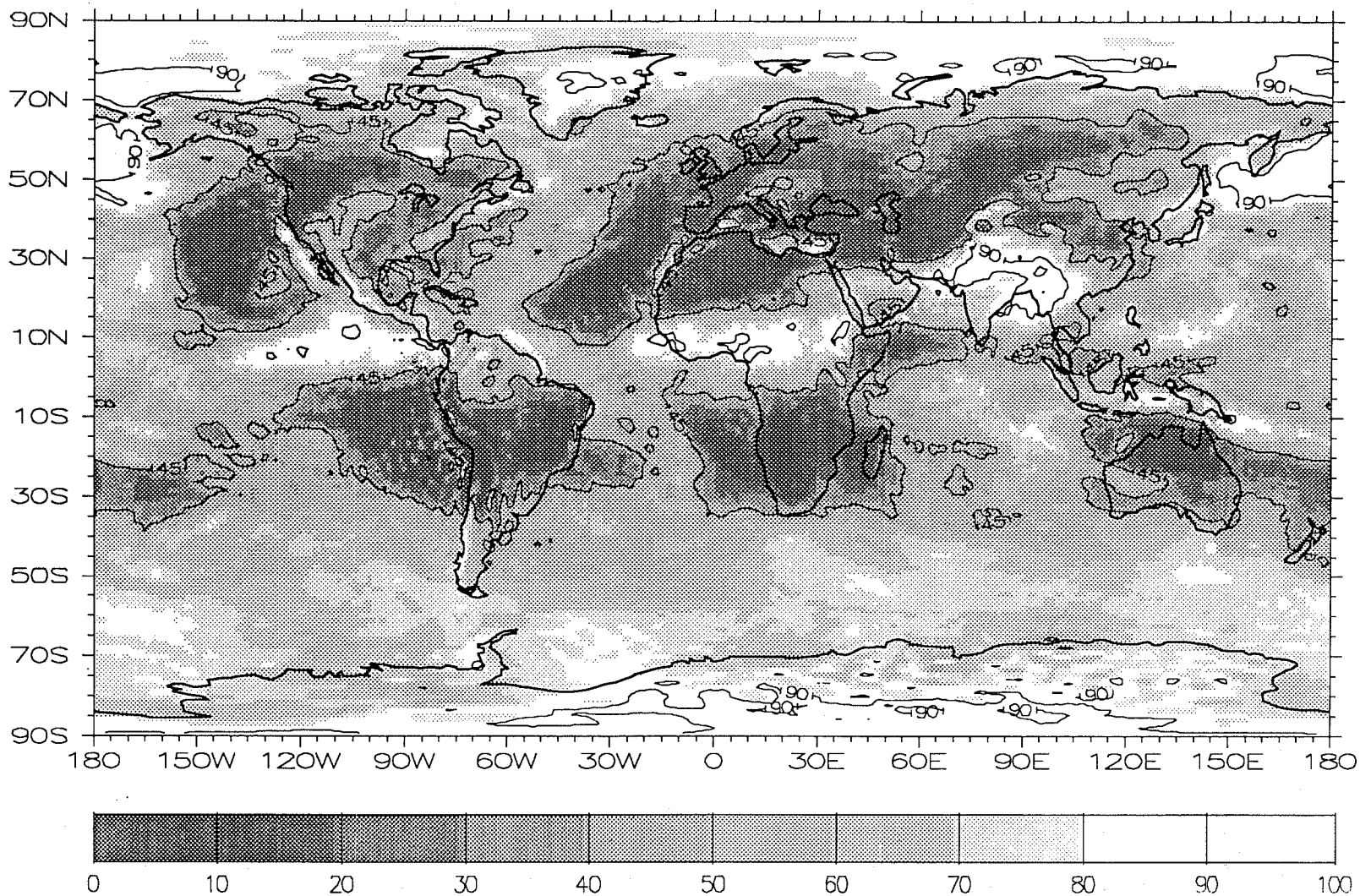

Figure 1b: The mean total cloudiness during the last 30 days of a T106 90-day perpetual July integration (%).

higher resolution. Thus it could be argued that an intercomparison of the cloud forcing from different models or from different resolutions might not be particularly informative because other areas of missing data will not be the same. The question of sample size also has to be considered and as yet the available literature gives no such information for the ERBE data. For model intercomparison, it is possible also that the sampling may be dependent on the type of cloud scheme used in a model. An "on/off" cloud scheme may show a greater incidence of clear skies than a fractional cloud scheme.

3.2. Length of time mean

It is clear from the description of Method I that it is only valid in a time mean sense and cannot be used to identify the instantaneous cloud forcing. It will also be dependent on the length of the time mean. The longer the averaging period the more likely it is that a pixel will eventually experience clear skies so that the areas of missing data should become smaller. Figure 2 shows the number of missing data for each latitude row of the T106 model for 10, 30 and 90 day averaging periods. There are substantial differences between the distributions based on 10 and 30-day averaging periods at most longitudes. With an increase in the averaging period to 90 days, the decrease in the number of missing data is less marked, reflecting the persistent nature of the ITCZ, the clouds over the Himalayan plateau and the status over the cloud waters of the North Pacific. These results suggest that a 30-day average is the minimum necessary to remove the effects of the transient features such as the Southern Hemisphere depression belt. Averaging over periods longer than 30 days is unrealistic because of the changing solar declination. The dependence of the cloud forcing determined from Method I on the length of the averaging period must be seen as another disadvantage both for model intercomparison and validation.

3.3. Diurnal bias in sampling

The diurnal variation in convective activity over the tropical continents has been well documented (e.g., Minnis and Harrison, 1984; Harrison et al., 1988). Typically, over land, it shows a peak in cloudiness in the afternoon with a minimum in the early hours of the morning. This suggests that a diurnal bias in the sampling, particularly for the shortwave cloud forcing, might be a problem with Method I. Figure 3(a)-3(d) shows the missing data for the T106 model perpetual July for days 61 to 90 at four times of the day, based on 00, 06, 12 and 18 GMT, respectively. These distributions are thus based on 30 samples each rather than 240 samples as used for the full time

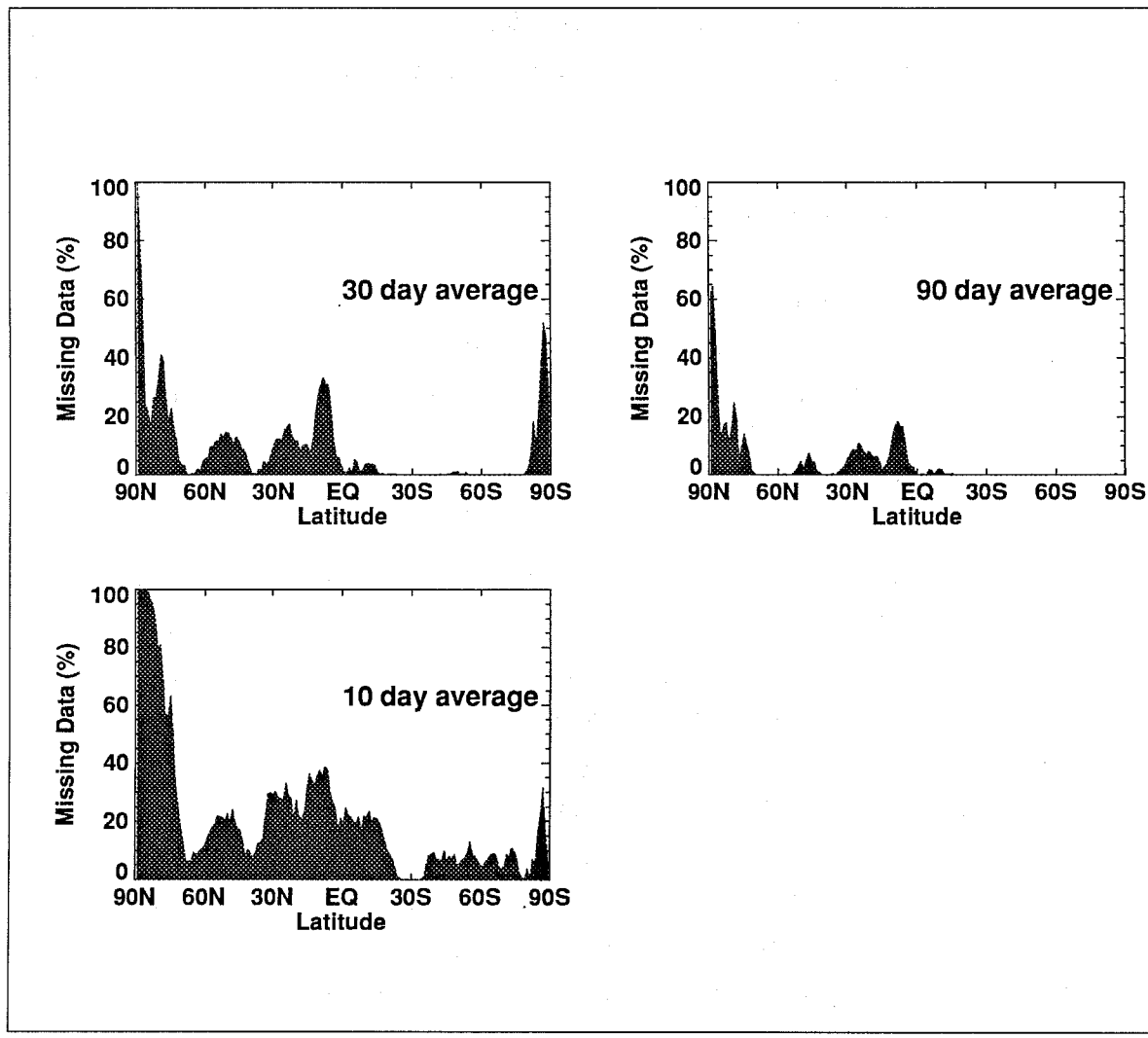

Figure 2: The number of missing data in percent for each latitude row of the T106 model for 10, 30 and 90 day avering periods.

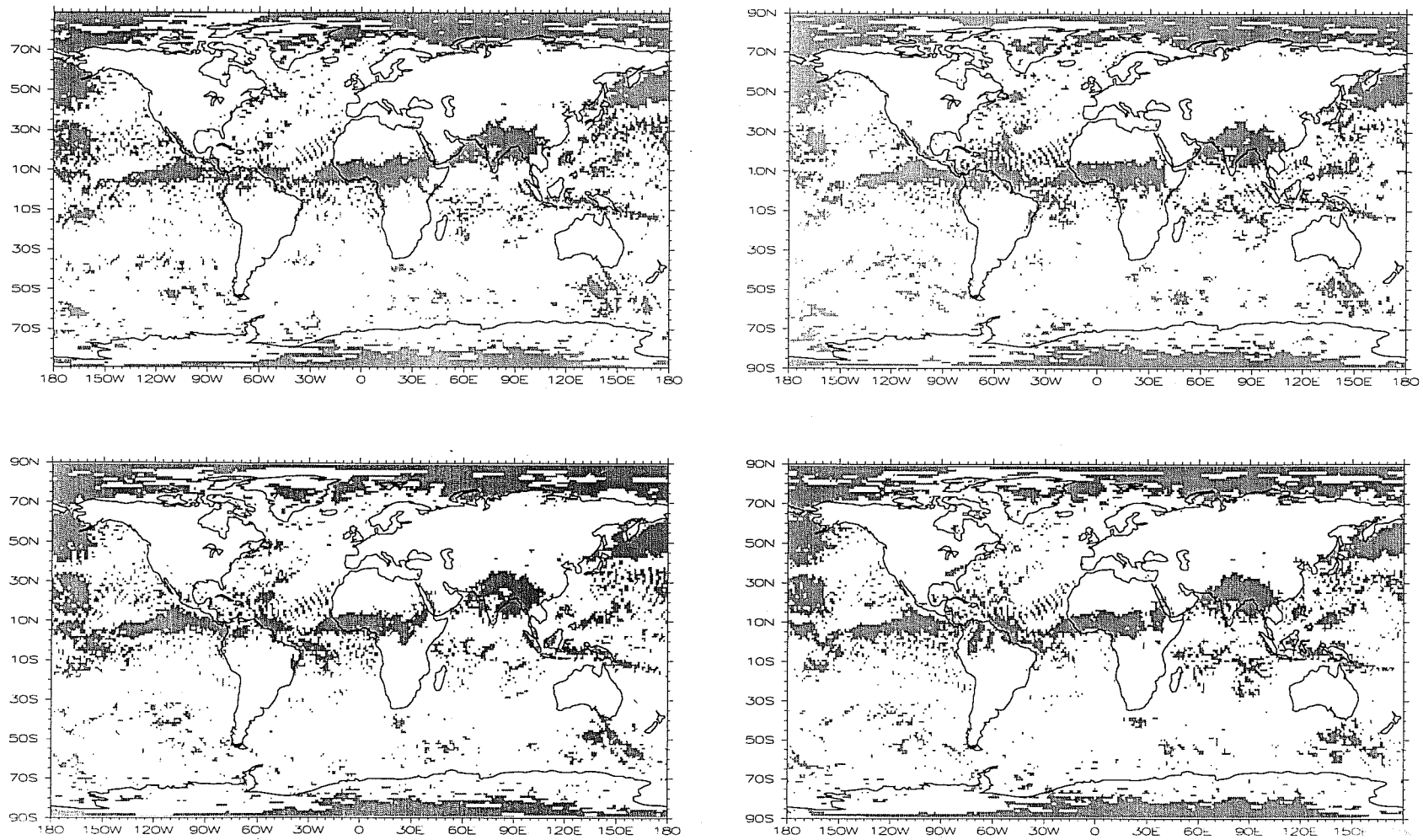

Figure 3: The missing data for the perpetual July T106 model simulation at 00 [Fig. 3(a) upper left], 06 [Fig. 3(b) upper right], 12 [Fig. 3(c) lower left] and 18 GMT [Fig. 3(d) lower right].

means shown in Figure 1. The areas of missing data are thus more extensive partly because of the smaller sample size. However, the importance of the diurnal cycle can be clearly seen particularly over South America. While Figure 1(a) shows very little missing data over the Amazon Basin, Figure 3(d) shows the development of more substantial areas of missing data at 18GMT associated with the onset of daytime convection. Thus the clear sky flux and hence the shortwave cloud forcing will be biased towards early morning or late afternoon values and the peak forcing near noon will not be properly sampled. The longwave cloud forcing is likely to display a diurnal bias also, but in a much less marked sense, through the diurnal variation in the land surface temperature. The results shown in Figure 3 are for July conditions; it is diurnal bias is larger in January when the convection over South America and South Africa is more extensive as shown in Figures 4(a)-4(d) for 00, 06, 12 and 18 GMT, respectively.

It is evident from the above discussion that the cloud forcing determined from Method I will depend on whether a model includes a diurnal cycle or not. Similarly it may also depend on the model's convection and cloud parameterization schemes and the response of those schemes to the diurnal variation in surface heating. Harshvardhan et al. (1989) have noted that the cloud forcing in the UCLA/GLA GCM, calculated using Method I, is influenced by that model's tendency to produce more cloud at night.

3.4. Cloud shortwave forcing: Flux method vs. albedo method

The shortwave cloud forcing computed using Method I for the T106 model is shown in Figure 5a. It is derived from monthly averaged fluxes, i.e.,

$$CSF = Q_{total} - Q_{clear} \tag{5}$$

where Q_{total} is the mean over the 240 samples and Q_{clear} is the mean over the clear sky samples only. The extreme negative and positive values are artifacts of the diurnal sampling problem already discussed. While the global mean shortwave forcing of -44.0 W m^{-2} is reasonable, the regional details of the two dimensional distribution are clearly not. The excessive negative values occur because the clear sky flux is only sampled near noon, with the consequence that the time averaged clear sky flux is an overestimation of the true daily averaged clear sky flux. similarly, there are also extreme positive values for the forcing (not shown in Figure 5(a)) which are due to the clear sky flux only being sampled either in the early morning or late afternoon, thus

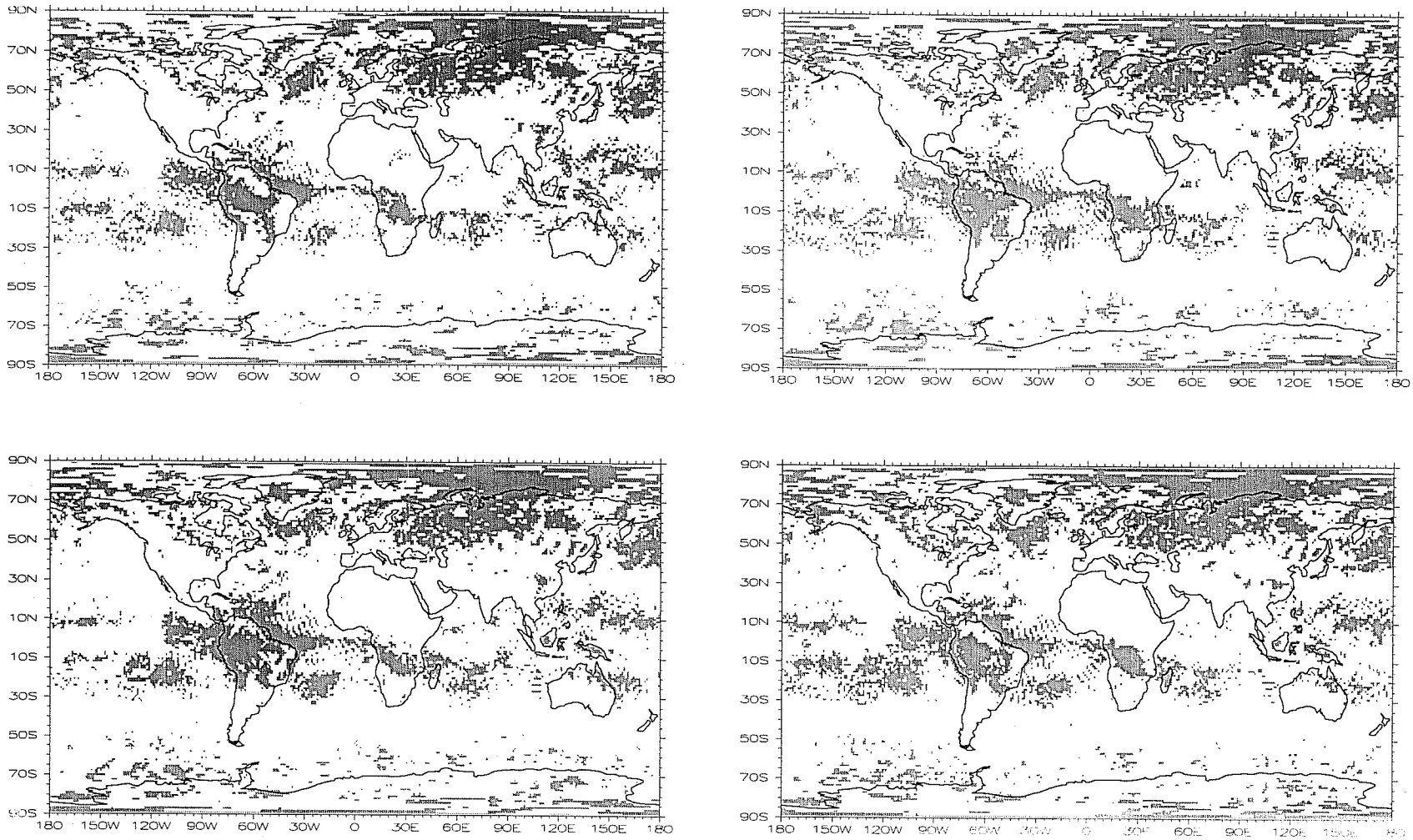

Figure 4: The missing data for the perpetual January T106 model simulation at 00 [Fig. 4(a) upper left], 06 [Fig. 4(b) upper right], 12 [Fig. 4(c) lower left] and 18 GMT [Fig. 4(d) lower right].

giving a value which is unrealistically small and hence implying a large, positive shortwave forcing. It is interesting to note that these extreme values of shortwave cloud forcing are located close to areas of missing data and are coincident with the areas of low percentage incidence of clear skies (generally less than 10%) shown in Figure 1(a).

The combination of the areas of missing data and the extreme values in regions of poor sampling would seem to make Method I impossible to use for the shortwave cloud forcing, particularly in a model which incorporates a diurnal cycle. However, some of the diurnal sampling problems can be overcome by resorting to the use of clear and cloudy sky albedos rather than fluxes. In this case the shortwave cloud forcing (CFS) becomes:

$$CFS = (\alpha_{total} - \alpha_{clear}) Q_{in} \qquad (6)$$

where α is the planetary albedo and Q_{in} the average incoming shortwave flux at the top of the atmosphere. As for fluxes, α_{total} is evaluated over the 240 samples whereas α_{clear} is the mean over the clear sky sample only. The diurnal variation in the solar radiation is thus effectively removed by the use of the time averaged insolation. The shortwave cloud forcing computed using the albedos rather than the fluxes is shown in Figure 5(b). The extreme values are absent and the main drawbacks of Method I are now the areas of missing data.

The problem of diurnal bias has not been completely resolved however, because the surface albedo over the oceans is a function of solar zenith angle. Starting from a low generic surface albedo ($\alpha_s = 0.07$), the radiation scheme produces a much higher value for the clear sky planetary albedo over the ocean at low solar elevation (0.169 for Q - 85°) than it does for high solar elevations (0.086 for Q = 5°). Thus if clear sky situations only occur early in the morning just after sunrise or late in the afternoon just before sunset over a given area, the resultant mean clear sky albedo will be biased towards high values. The clear sky albedo over the tropical belt (between 30°S and 30°N), calculated using Method I, is not a uniform field over the oceans (Figure 5(b)). In regions where the percentage incidence of clear skies is small (Figure 1(a)), the clear sky albedo tends to be noisy, indicative of the sampling being biased towards a particular time of day. The pattern of higher values repeating itself eight times over the globe south of 10°S simply reflects the fact that the instantaneous radiation fields in our perpetual July integrations have been stored every 3 hours. Then the "mean" field produced here is the superimposition of 240 fields but including the sun at only eight

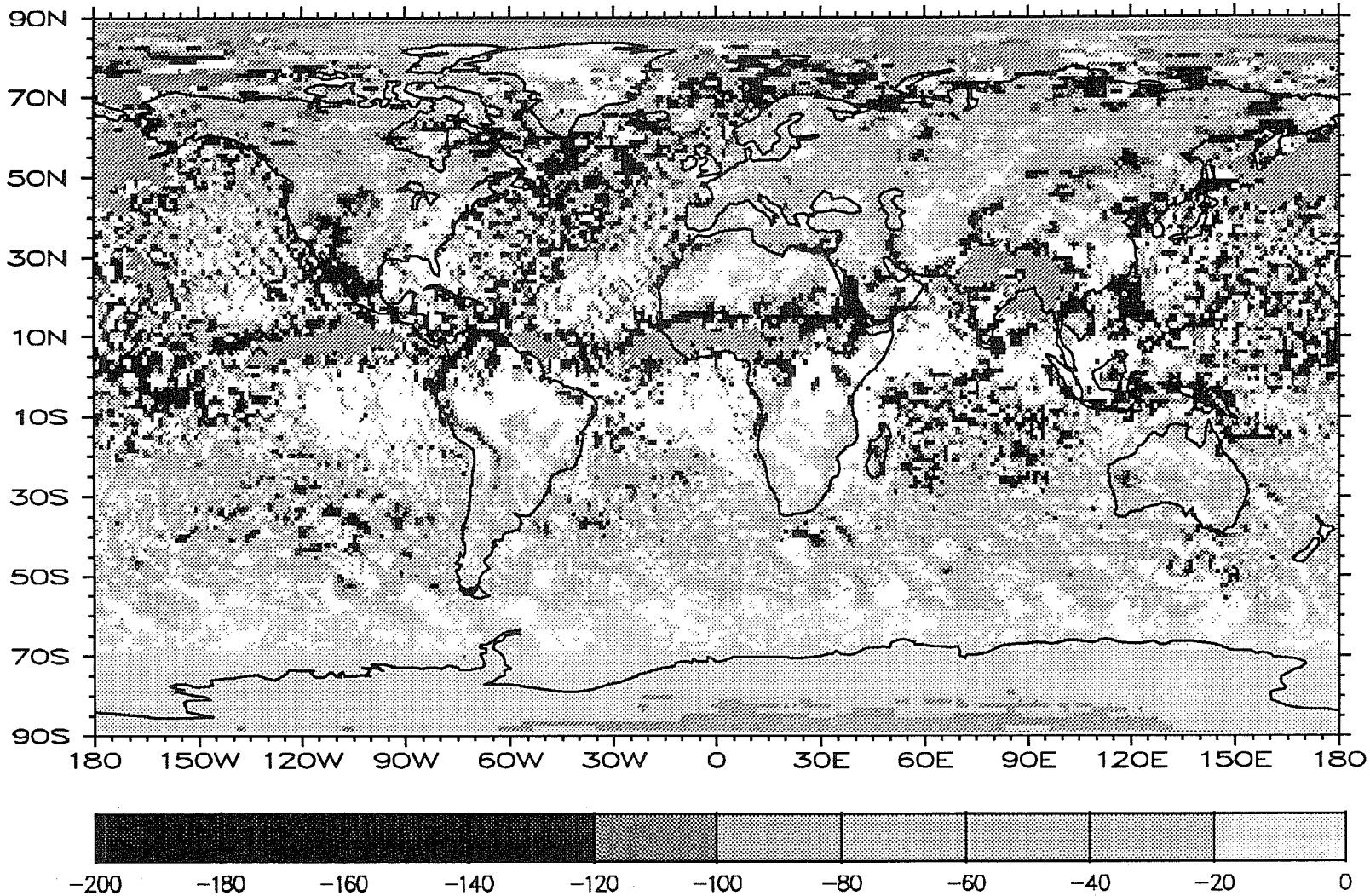

Figure 5a: The shortwave cloud forcing computed using Method I from monthly averaged fluxes (Wm^{-2}).

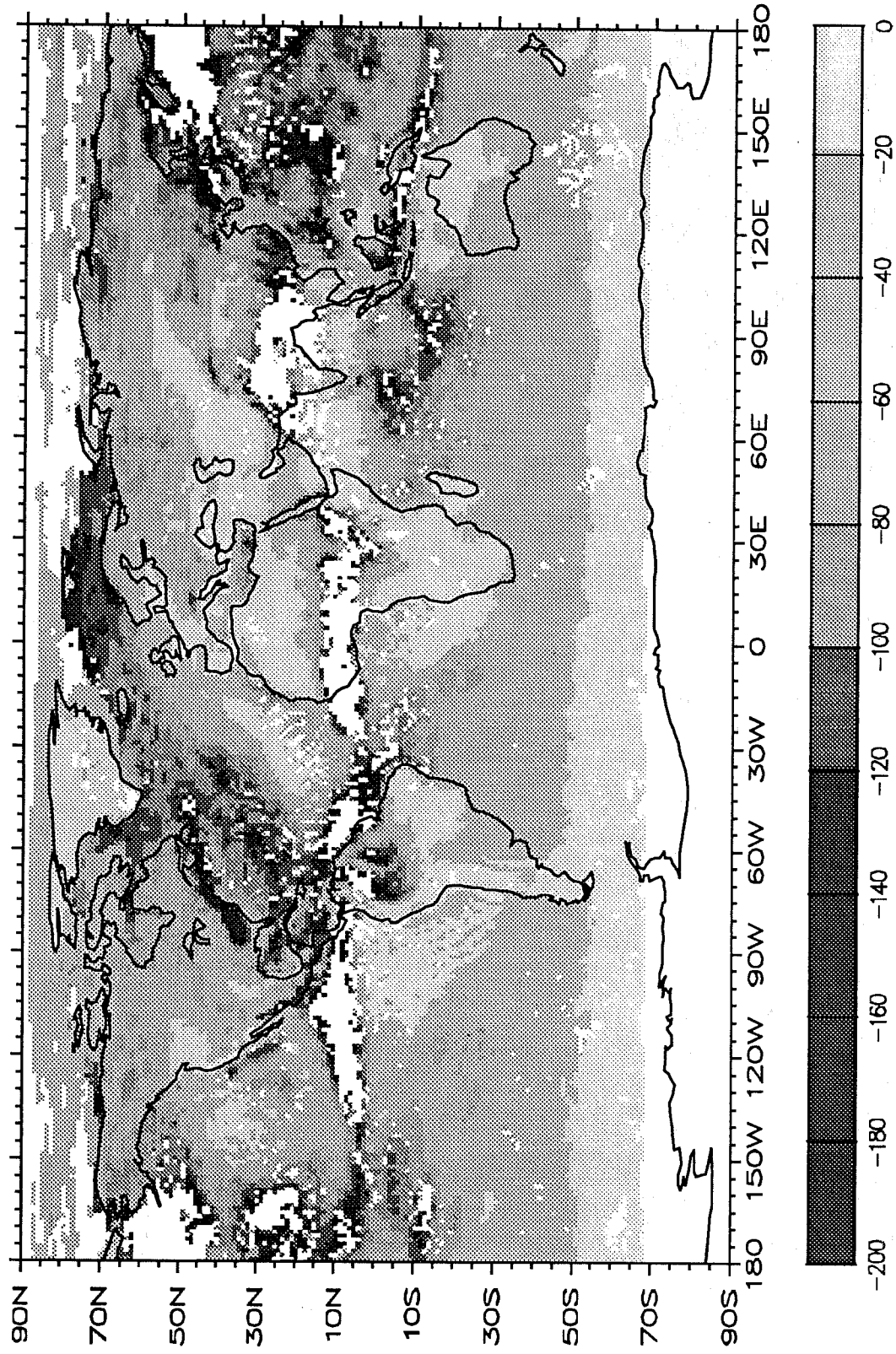

Figure 5b: The shortwave cloud forcing computed using Method I from monthly albedos (Wm^{-2}).

different locations. Such a pattern would also appear with Method II clear sky albedo. The only way of overcoming this would be to store accumulated fluxes between sampling times.

Strictly speaking, the cloud forcing should be computed using fluxes and not albedos so that the correct weighting can be given to the cloud forcing. The fact that Method I cloud forcing cannot be computed in this way demonstrates its unsuitability for assessing the diurnal variation in the forcing. It is important that modellers should appreciate the difference between the albedo and flux calculations when using Method I. For intercomparison, it is clearly desirable that, if Method I is used, it should be based on albedo to minimize the problems of diurnal sampling.

3.5. Cloud longwave forcing

Figure 6 shows the longwave cloud forcing using Method I. The longwave forcing is defined as:

$$CLF = (F_{clear} - F_{total}) \tag{7}$$

where F_{clear} and F_{total} are are the longwave fluxes at the top of the atmosphere and their clear and total components are calculated in the same way as for Method I solar fluxes. Again the large regions of missing data in the general region of the ITCZ and in the North Pacific are significant. It is apparent that the regions of the largest longwave forcing are in the regions where the data is mostly missing.

4. METHOD II

4.1. Shortwave cloud forcing

The shortwave cloud forcing computed using Method II is shown in Figure 7. Comparison with Figure 5(b) confirms the result that the areas of missing data with Method I are coincident with the areas of greatest forcing. Thus Method I will underestimate the shortwave cloud forcing by a considerable amount.

4.2. Longwave cloud forcing

A similar result will apply to the longwave cloud forcing. Figure 8 shows the longwave cloud forcing computed using Method II. While the shortwave forcing is

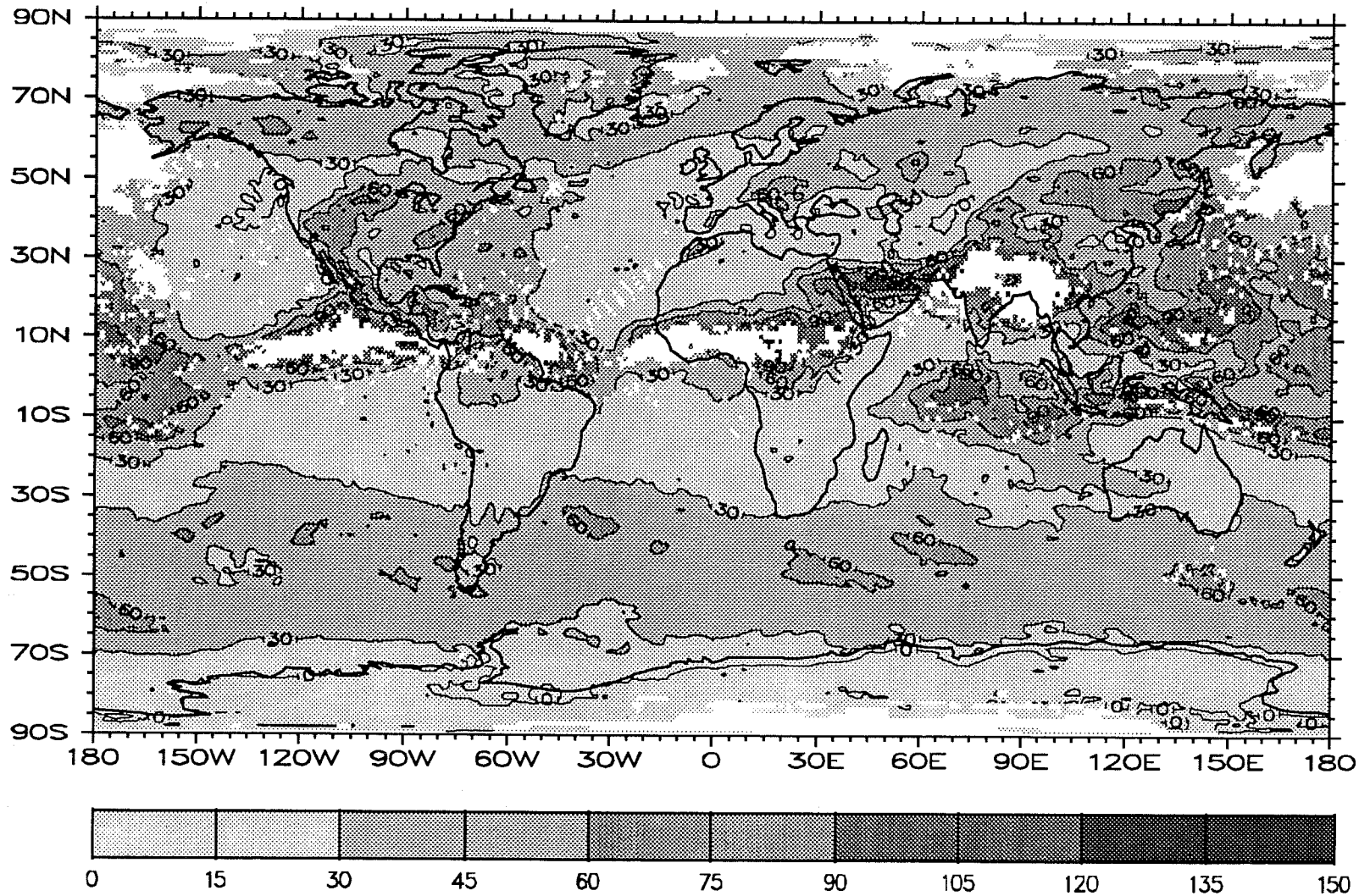

Figure 6: The longwave cloud forcing computed using Method I (Wm^{-2}).

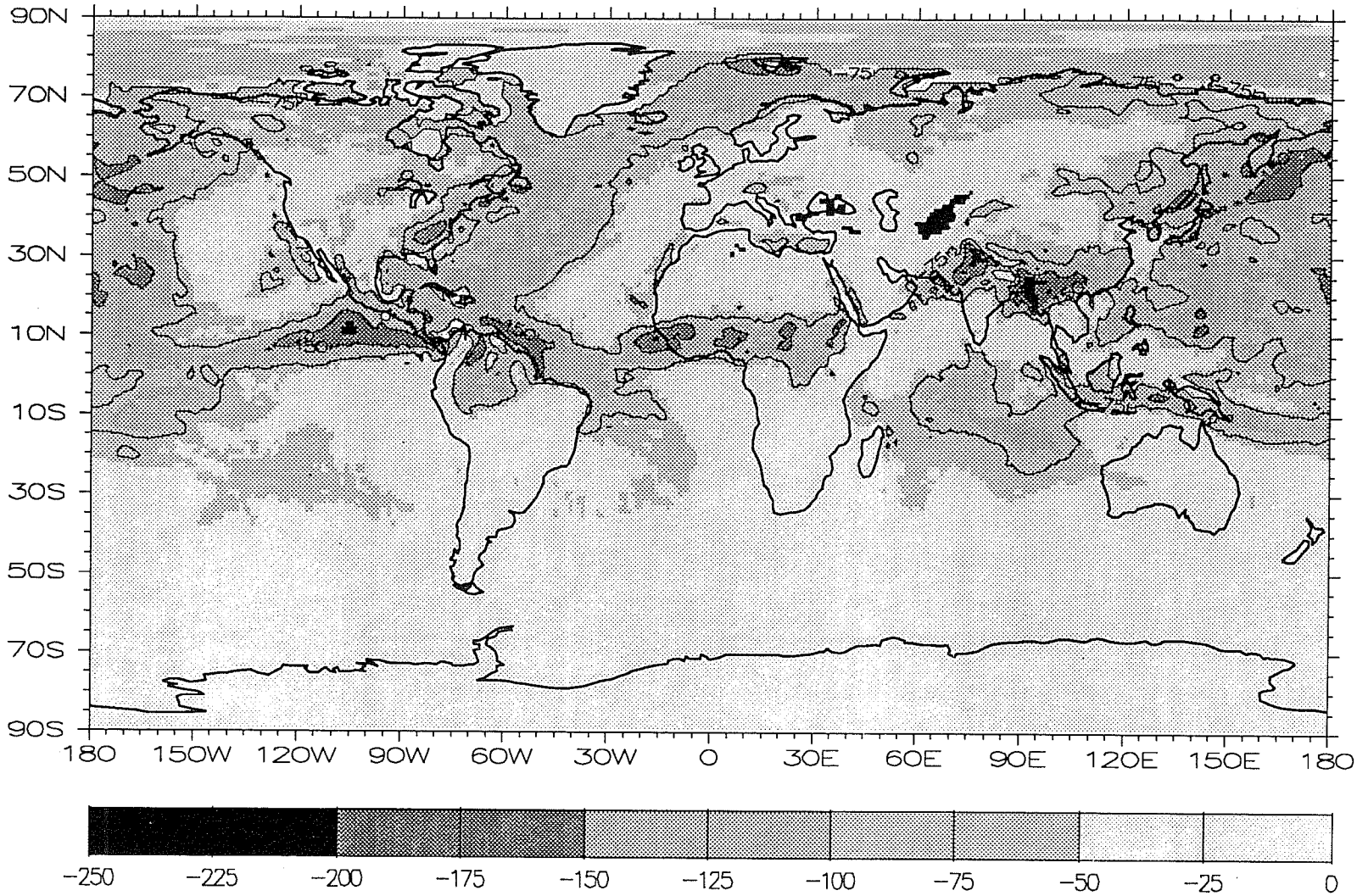

Figure 7: The shortwave cloud forcing computed using Method II (Wm^{-2}).

dominated by cloud amount, the cloud longwave forcing is dependent on cloud height as well as cloud amount. The colder the cloud radiating temperature relative to the temperature of the underlying surface, the greater the cloud longwave forcing. Thus as Figure 7 shows, the main areas of longwave forcing are associated with the dense cirrus clouds of the ITCZ. The low level status clouds of the North Pacific, important in the shortwave forcing, have little impact on the longwave forcing. The main differences between the missing data. As the comparison of Figures 6 and 7 show, the main areas of missing data are coincident with the regions of deep convection in the tropics, precisely where the longwave cloud forcing is large. Other small differences are evident, particularly over the continents of the summer hemisphere. These are due to sampling problems in Method I such that the clear sky values are not representative of the same atmospheric and surface conditions. Over land, such as East Asia and the United States, they will tend to be associated with warmer surface temperatures due to greater solar heating with clear skies. It is possible that some of this tendency to overestimate the clear sky longwave flux will be compensated if the diurnal bias is such as to give more sampling at night. However, the difference over the Southern Hemisphere oceans where there can be no diurnal bias or surface temperature effects (as SST is fixed at climatological values), must be related to the tendency for clear sky conditions to contain less water vapor and thus give a higher clear sky flux than for cloudy conditions. Since Method I only samples the clear sky atmospheric state then it will be biased towards drier conditions.

4.3. Intercomparison discussion

The advantages of Method II are substantial when the purpose is model intercomparison or analysis of cloud feedback. Differences in the cloud forcing between models can be directly related to differences in the physical parameterizations. Because Method II is free from any sampling biases, the clear sky fluxes between models can readily be compared. On the other hand, Method I is dependent on a host of characteristics specific to each model, which include the horizontal resolution, the type of cloud parameterization scheme employed (fractional or "on/off"), the presence of a diurnal cycle, the length of the averaging period, the frequency of model history writes and so on.

5. METHOD III

Results of Method III are very similar to those from Method II as shown in the comparison of zonal mean CSF and CLF by all three methods in Figure 9. However,

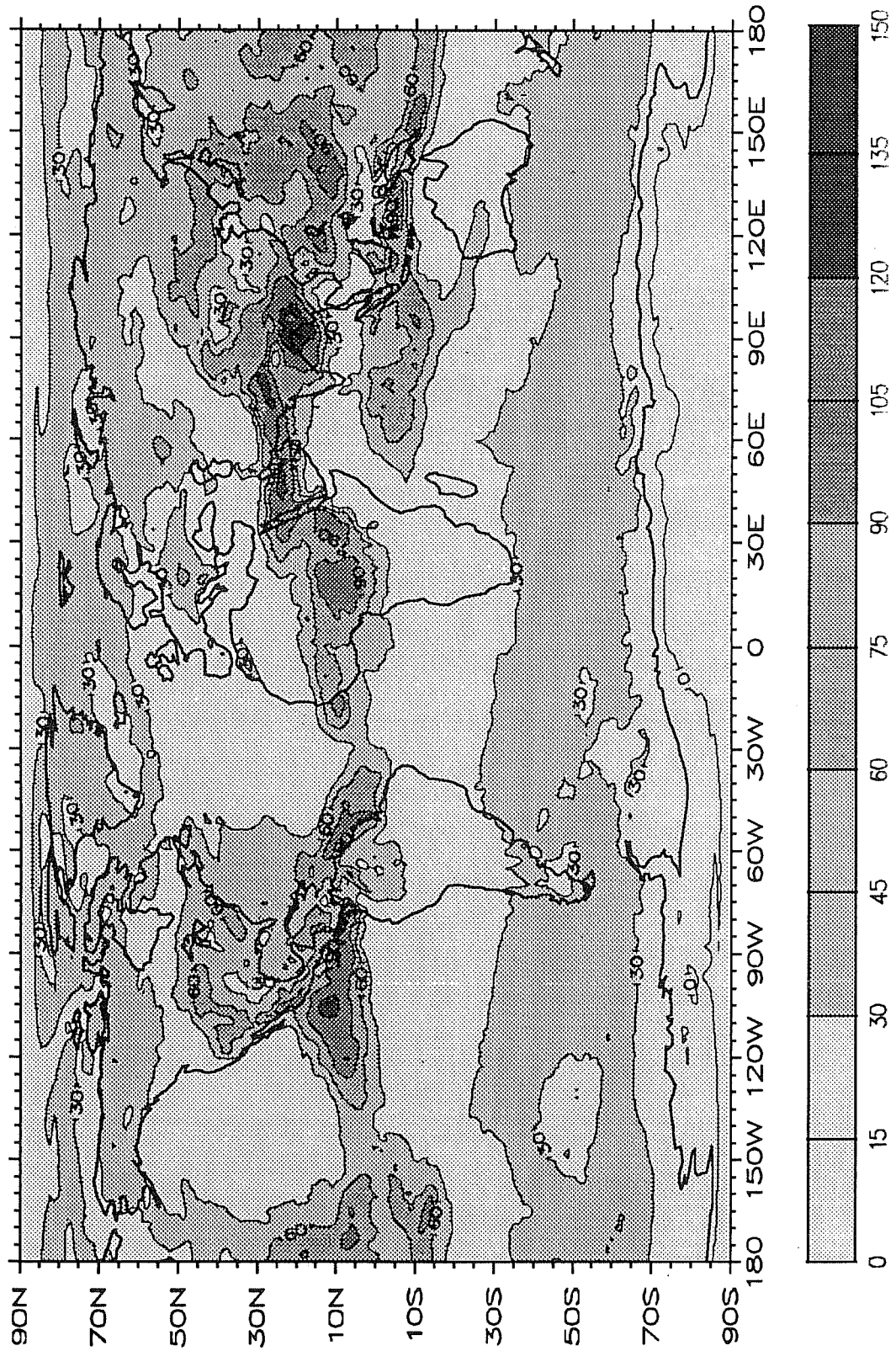

Figure 8: The longwave cloud forcing computed using Method II (Wm^{-2}).

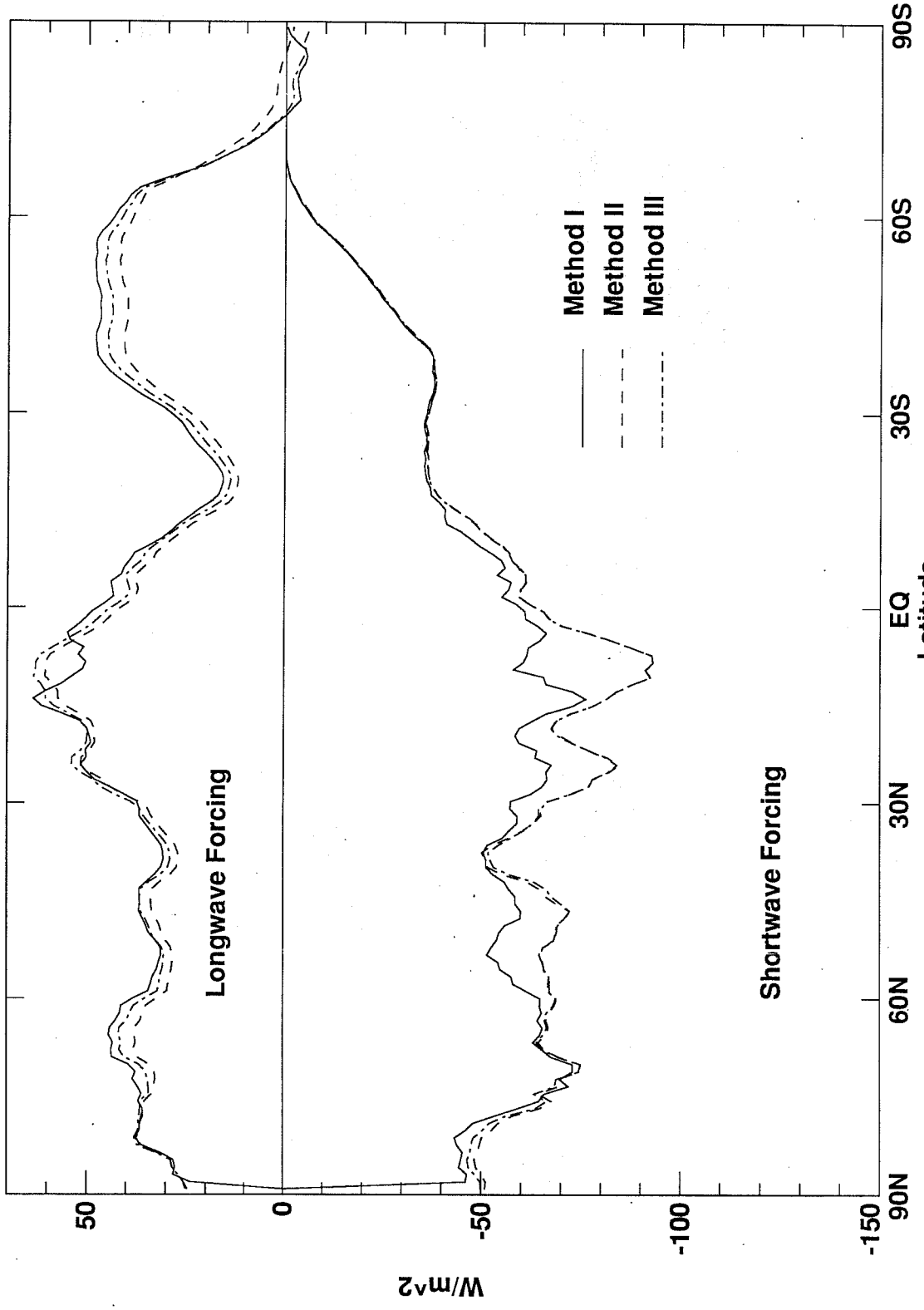

Figure 9: The zonally averaged shortwave (bottom) and longwave (top) cloud forcing computed using Methods I, II, and III (Wm^{-2}).

this result is in fact very model-dependent. In the ITCZ, Methods II and III give similar results simply because the ECMWF cloud scheme (Slingo, 1987) does not allow a 100% convective cloud cover. Instead a 80% maximum is assumed so that even in the areas of permanent convection (the white areas of Figure 1(a) with Method I) there is always a clear-sky fraction in the grid-box. In contrast, the cloud scheme allows for 100% cloud cover for the stratiform clouds and such overcast clouds are often found in the storm tracks.

Figure 10 shows the global CLF differences between Method III and Method II. In general, Method III slightly overestimates cloud forcing (white areas) primarily from areas that produce large-scale cloud cover. Method III does not calculate fluxes for completely overcast regions and thereby biases the results to more clear areas that have a reduced water vapor amount thus allowing more longwave radiation to space - thus higher values for clear sky and longwave forcing. Except in the high southern latitudes, the zonal average fluxes (not shown) are consistently 2 to 4 Wm^{-2} higher for Method III than for Method II .

To illustrate that point, we show in Figure 11 the incidence of overcast (cloud fraction of 1) "observations" during the 30-day period. Only the storm tracks of the Southern Hemisphere display some large occurrence likely to modify substantially the weighting of the clear-sky flux in Method III relative to Method II.

One can think of a cloud scheme where overcast cloud is never permitted (the NCAR CCM cloud scheme). In that case, Method II and III results should be very close to each other. One can also think of a on-off cloud scheme (cloud cover is either 0 or 1). if some areas remain cloudy during the whole period, they will show as missing clear-sky "observations" exactly as in Method I. In some respect, Method III is in between Methods I and II. However, for model intercomparison of cloud forcings (not comparison of model cloud forcings with satellite derived cloud forcings), Method II is the only consistent one.

6. SENSITIVITIES AND CLOUD FEEDBACK

It is now interesting to study how the various determinations of the clear-sky fluxes influence the climate sensitivities in the framework of the surrogate climate change experiments of Cess et al. (1989). In the following, we closely follow the notation of that paper. We define a clear-sky sensitivity λ_c and a total sensitivity λ from the following expressions

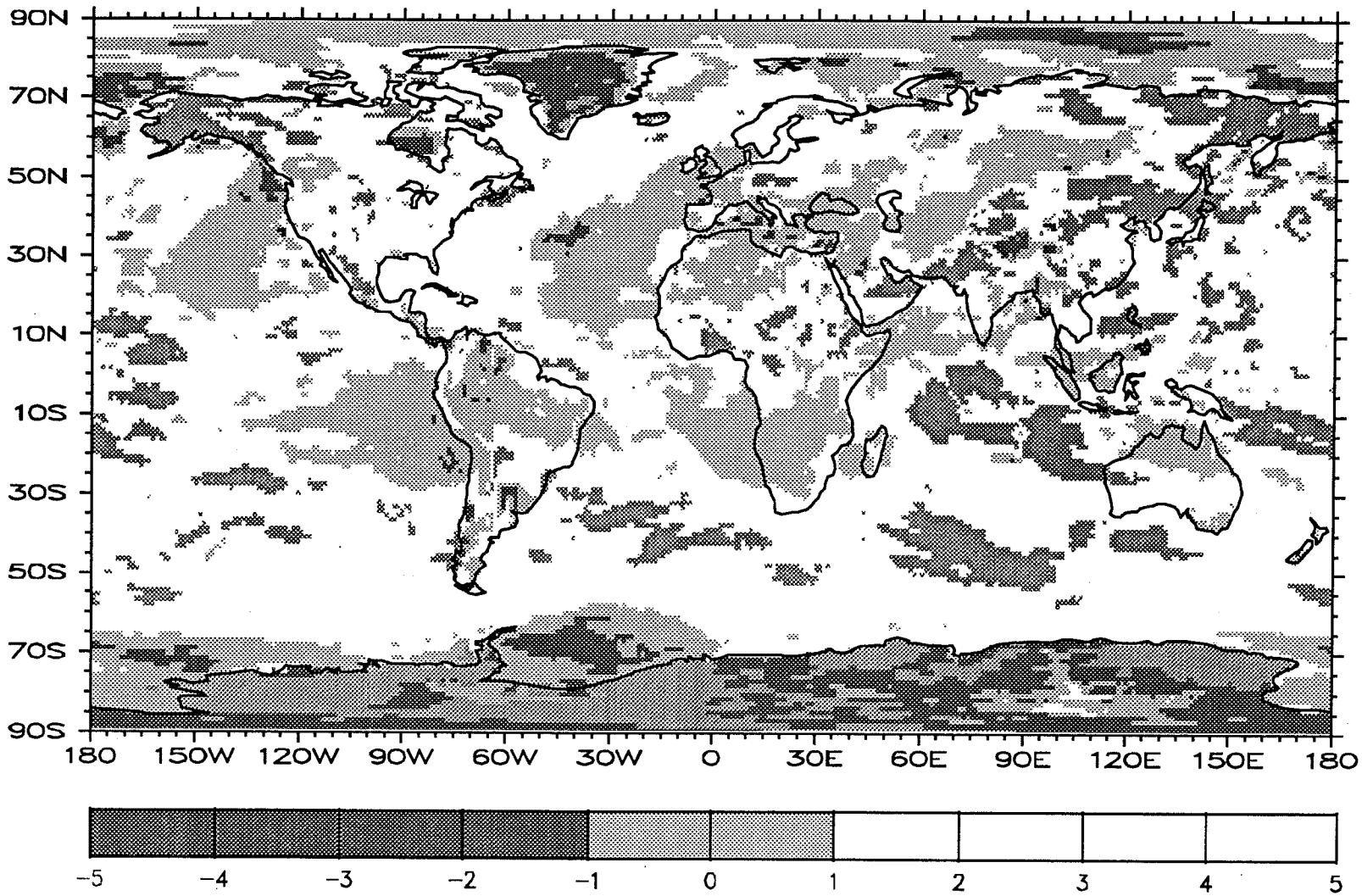

Figure 10: The difference (Method III - Method II) in longwave cloud forcing computed using Methods II and III (Wm^{-2}).

$$\lambda = \frac{1}{\frac{\Delta F}{\Delta T_s} - \frac{\Delta Q}{\Delta T_s}} \qquad (8)$$

where ΔF is the change in clear sky (total) outgoing longwave flux, ΔQ the change in clear sky (total) absorbed solar radiation and ΔT_s the change in global mean surface temperature.

Table 1 lists the globally averaged values of all relevant fluxes in the control experiment (T106 perpetual July, fixed climatological sea surface temperature) and the differences in the same quantities between a SST + 2K and a SST - 2K experiments. Clear-sky fluxes and corresponding cloud forcings are reported as obtained by Method I (albedo), Method II and Method III.

6.1. Impact of resolution

Cess et al. (1989) presented sensitivities and cloud feedbacks obtained by various models with various resolutions. Among these models, the ECMWF model is one of two models showing a negative cloud feedback. Then, a question rise whether such a result is robust. Another way of addressing the same question is whether results obtained in the previous sections at T106 still hold at lower resolution. This question is highly relevant as some models seem to have difficulties to cope with higher resolution, at least regarding their distribution of humidity, and therefore cloudiness and corresponding fields (Kiehl and Williamson, 1990). Another study (Morcrette et al., 1991) documents the details of the sensitivity to horizontal resolution of the cloud and radiation fields in the ECMWF model. Here, it is sufficient to say that the humidity, cloudiness and radiation fields are quite robust features in the ECMWF model, as can be seen in a comparison of T106 vs. T21 global means of radiation fields and cloud radiative forcings in Table 1. The zonal means of total cloudiness are shown in Figure 11(a) whereas Figures 11(b), 11(c) and 11(d) present the zonal means of the longwave, shortwave and net cloud forcings obtained with the various methods, respectively. The main result is that the negative cloud feedback of the ECMWF model in the surrogate climate change experiment appears to be invariant to changing horizontal resolution.

6.2. Impact on cloud feedback

The lower portion of Table 1 presents the changes (SST+2C) - (SST-2C) for the ECMWF model for T106 and T21. As with all of the other models in Cess et al.

Table 1: Global means of radiation parameters at the top of the atmosphere for two sets of experiments run at T106 and T21 horizontal resolution. Methods I, II and III refer to the method used for deriving the clear-sky fluxes and corresponding cloud forcings and sensitivities.

Control

	T106	T21
cloud amount (%)	53.11	55.93
surface temperature (C)	16.57	17.18
total OLR (Wm^{-2})	245.98	240.80
total absorbed SW (Wm^{-2})	234.81	235.81

	Method I		Method II		Method III	
	T106	T21	T106	T21	T106	T21
clear-sky OLR (Wm^{-2})	286.99	286.72	281.12	279.92	283.50	282.97
clear-sky abs SW (Wm^{-2})	286.02	285.96	287.39	287.46	287.197	287.09
longwave forcing (Wm^{-2})	38.41	43.84	35.14	39.11	37.52	42.15
shortwave forcing (Wm^{-2})	-43.96	-38.75	-52.59	-51.65	-57.05	-50.09
net cloud forcing (Wm^{-2})	-5.55	5.04	-17.45	-12.54	-19.53	-7.94

Changes (SST +2C) - (SST - 2C)

	T106	T21
cloud amount (%)	-1.95	-1.76
surface temperature (C)	3.40	3.47
total OLR (Wm^{-2})	5.66	7.63
total abs. SW (Wm^{-2})	-4.87	-5.05
λ ($Km^2 W^{-1}$)	0.32	0.27

	Method I		Method II		Method III	
	T106	T21	T106	T21	T106	T21
clear-sky OLR (Wm^{-2})	7.72	8.13	7.59	8.04	7.63	8.08
clear-sky abs SW (Wm^{-2})	-0.27	-0.07	0.54	0.66	0.64	0.70
longwave forcing (Wm^{-2})	1.49	0.29	1.94	0.41	1.97	0.44
shortwave forcing (Wm^{-2})	-3.20	-2.88	-5.41	-5.71	-5.28	-5.79
net cloud forcing (Wm^{-2})	-1.71	-2.58	-3.47	-5.31	-3.30	-5.35
λ_c ($Km^2 W^{-1}$)	0.44	0.42	0.48	0.47	0.45	0.47
$\lambda/\lambda_c = 1+\Delta CRF/G$	0.76	0.64	0.66	0.57	0.71	0.57

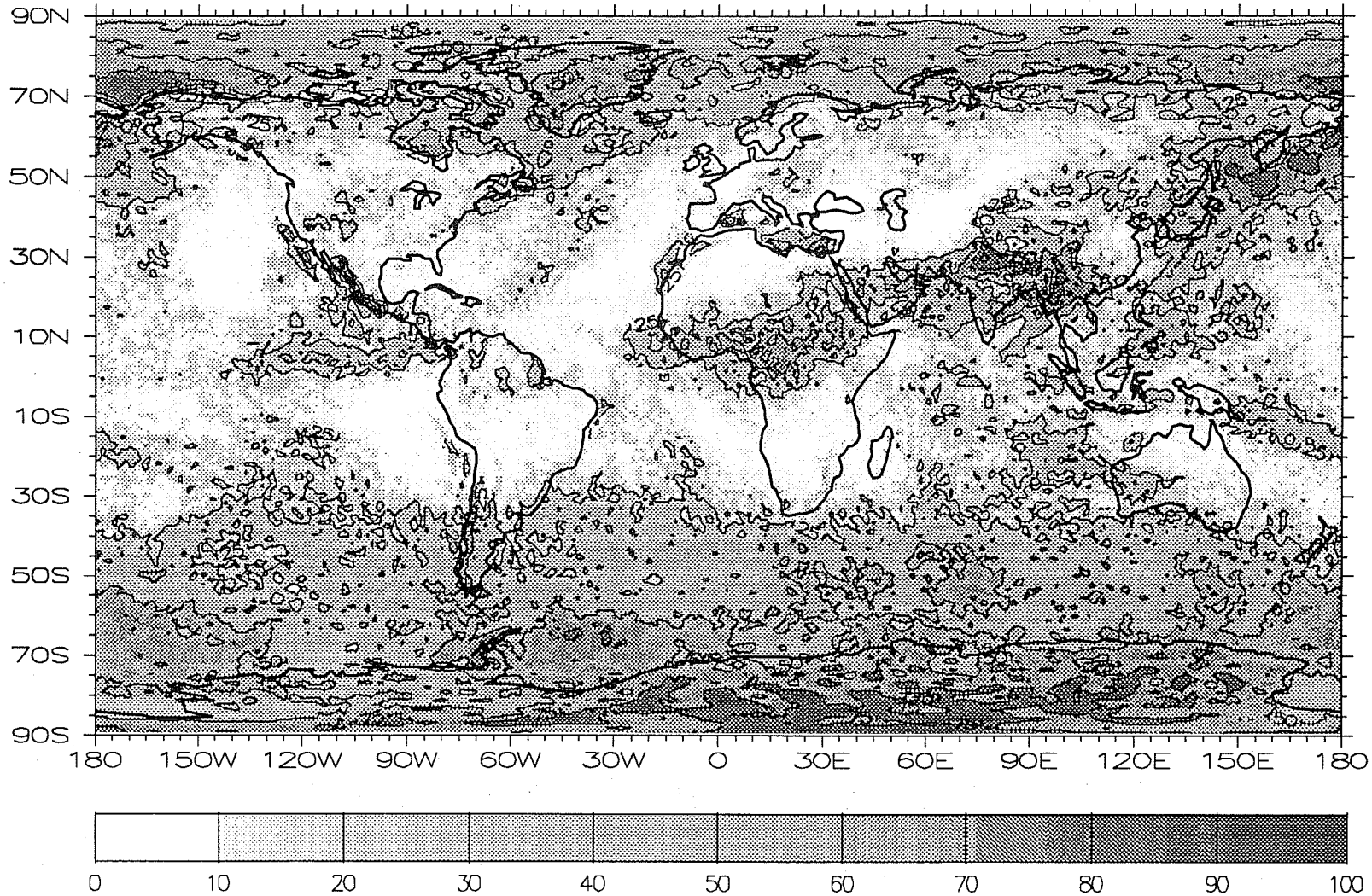

Figure 11: The incidence of overcast observations during the last 30 days of a T106 90-day perpetual July integration (%).

(1989), the total cloud amount decreased. The most interesting feature of the changes is the reduction of solar absorption for both resolutions. Although the T21 shows a somewhat larger reduction in absorption the shortwave feedback is nearly the same ($\Delta Q/\Delta T_S$ = -1.43 for T106 and -1.45 for T21). This apparently can be attributed to the increased liquid water in the warmer simulation and resulting increase in tropical cloud albedo. It is conceivable that the negative feedback could be the result of decreased cloud altitude which in turn would produce clouds with more liquid water and hence brighter. The net effect of this result is that $\lambda < \lambda_c$ and from Cess et al. this denotes a negative cloud feedback. The analysis of this is beyond the scope of this paper but in any case, it is significant and will require further research.

It is surprising that the method for determining longwave and shortwave cloud forcing does not appear to have a significant effect on the differences in global values. But as demonstrated above, in order to compare and validate models, Method I introduces large uncertainty in regions of most interest. This is of particular importance in the ECMWF model where it is suspected that the negative cloud feedback arises from regions that have significant missing data.

7. CONCLUSION

As noted by Kiehl and Ramanathan (1990), the cloud forcing approach (applied on satellite data with Method I) only produces diagnostics relevant to monthly mean time scales. While this is already a useful information, it is far from giving insight on the detailed interactions that link together the large-scale circulation, moist processes in particular convection, cloud and radiation. In that respect, Method II is, from a modeller's point of view, the only method able to properly document the diurnal cycle and day-to-day variability of the cloud radiative forcing. An intercomparison of climate models aiming at understanding the differences in sensitivities will have to address (among many other things) how these interactions are dealt with by the different models on a smaller spatial and shorter temporal scales (for example, diurnal cycle of ITCZ).

As shown in this study, only Method II allows a clear, simple cloud forcing definition without ambiguity that can readily be compared from model to model. Only Method II ensures that the temporal and spatial of the clear-sky "observations" is the same in any model. Method I, although discussed by Cess and Potter (1987) as being the closest in principle to the method used to derived cloud radiative forcing from satellite observations suffer from a number of problems. The results are highly dependent on the number and location of missing clear-sky "observations" that

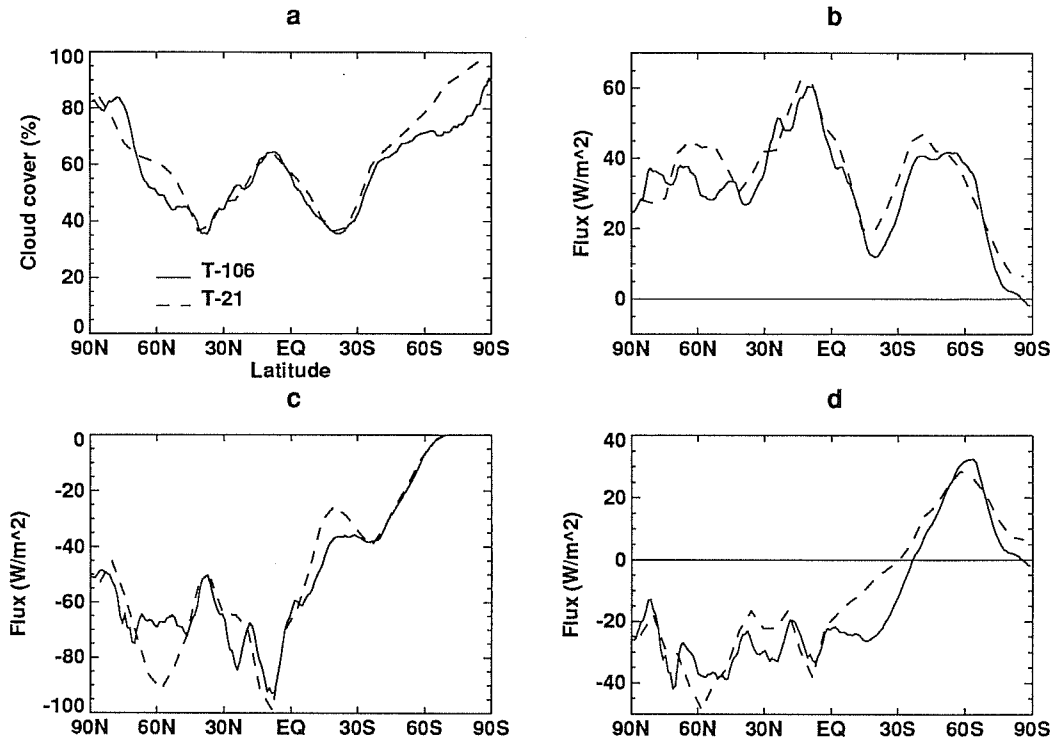

Figure 12: [Fig. 12(a)]The zonally averaged total cloudiness during the last 30 days of a T106 (solid) and T21 (dashed) 90-day perpetual July integrations (%).[Fig. 12(b)] The zonally averaged longwave cloud forcing during the last 30 days of a T106 and T21 90-day perpetual July integrations (Wm^{-2}). [Fig. 12(c)] The zonally averaged shortwave forcing during the last 30 days of a T106 and T21 90-day perpetual July integrations(Wm^{-2}).[Fig. 12(d)] The zonally averaged net cloud forcing during the last 30 days of a T106 and T21 90-day perpetual July integrations (Wm^{-2}).

generally occur in areas where the cloud forcing is large. Therefore Method I cloud forcings are likely to be underestimated. Moreover, different models will have a different spatio-temporal distribution of these areas of missing clear-sky observations, which itself depends on the length of the "observation" period. Method 3 is in fact closer to the method used to derived the cloud radiative forcing from the ERBE observations in the so-called S4 format. However, results from Method III are also model-dependent through the cloud generation scheme.

In simulating a climate change, the response of cloud forcing from the resulting cloud property modification cannot be determined using Method I. For regions lacking clear-sky grids such as in the ITCZ, cloud optical or height changes will have no impact on cloud forcing calculated using Method I. In another model study Mitchell et al. (1989) demonstrated that changing cloud type and properties or vertical structure could modify cloud feedback significantly.

Furthermore, using either Methods I or III, a correct comparison with cloud forcing derived from ERBE observations would require that the clear sky fluxes be processed in a way that is consistent with that done on ERBE measurements to properly account for the diurnal cycle. Such an effort is unjustified as a proper treatment of the diurnal cycle is built in when the clear-sky fluxes are derived from Method II.

ACKNOWLEGMENTS

The authors would like to thank Dr. W. Lawrence Gates for his support in this project, Mr. John L. Stout for helping with the simulations, the National Energy Research Supercomputer Center for computational support and Linda Kennedy for helping with the manuscript. This was performed under the auspices of the Atmospheric and Climate Research Division, U.S. Department of Energy contract W-7405-ENG-48 to Lawrence Livermore National Laboratory.

REFERENCES

Alexander, R.C., and R.L. Mobley, 1976: Monthly average sea-surface temperature and ice-pack limits on a 1o global grid. *Mon. Wea. Rev.*, **104,** 143-148.

Brooks, D.R., E.F. Harrison, P. Minnis, J.T. Suttles, and R.S. Kandel, 1986: Development of algorithms for understanding the temporal and spatial variability of the Earth's radiation balance. *Rev. Geophys.*, **24,** 422-438.

Cess, R.D., and G.L. Potter, 1987: Exploratory studies of cloud radiative forcing with a general circulation model. *Tellus,* **39A,** 460-473.

Cess, R.D., G.L. Potter, J.-P. Blanchet, G.J. Boer, S.J. Ghan, J.T. Kiehl, H. Le Treut, Z.X. Li, X.-Z. Liang, J.F.B. Mitchell, J.-J. Morcrette, D.A. Randall, M.R. Riches, E. Roeckner, U. Schlese, A. Slingo, K.E. Taylor, W.M. Washington, R.T. Wetherald, and I. Yagai, 1989: Interpretation of cloud-climate feedback as produced by 14 atmospheric general circulation model. *Science,* **245,** 513-516.

Coakley, J.A., Jr., and D.G. Baldwin, 1984: Towards the objective analysis of clouds from satellite imagery data. *J. Climate Appl. Meteor.,* **23,** 1065-1099.

Harshvardhan, D. A. Randall, T. G. Corsetti, and D. A. Dazlich, 1989: Earth radiation budget and cloudiness simulations with a general circulation model. *J. of Atmosph. Sci.*,**46**,No. 13, 1922-1942.

Harrison, E.F., D.R. Brooks, P. Minnis, B.A. Wielicki, W.F. Staylor, G.G. Gibson, D.F. Young, F.M. Denn, and the ERBE Science Team, 1989: First estimates of the diurnal variation of longwave radiation from the multiple-satellite Earth Radiation Budget Experiment (ERBE). *Bull. Amer. Meteor. Soc.,* **69,** 1144-1151.

Hollingsworth, A., A. Lorenc, M.S. Tracton, K. Arpe, G. Cats, S. Uppala, and P. Kallberg, 1985: The response of numerical weather prediction systems to FGGE level II-b data. Part I: Analyses. *Quart. J. Roy. Meteor. Soc.,* **111,** 1-66.

Kiehl, J.T., and D. Williamson, 1990: Comparison of cloud forcing derived from the Earth Radiation Budget Experiment with that simulated by the NCAR Community Climate Model. *J. Geophys. Res.*,**95**, No. D8, 11,679-11,698.

Mitchell, J. B. F., C. A. Senior and W. J. Ingram, 1989: CO_2 and climate: a missing feedback? *Nature*, **341**, 132-134.

Morcrette, J.-J., 1990: Impact of changes to the radiation transfer parameterizations plus cloud optical properties in the ECMWF model. *Mon. Wea. Rev.,* **118,** 847-873.

Ramanathan, V., 1987: The role of Earth Radiation Budget studies in climate and general circulation research, *J. Geophys. Res.,* **92,** 4075-4095.

Ramanathan, V., R.D. Cess, E.F. Harrison, P. Minnis, B.R. Barkstrom, E. Ahmad, and D. Hartmann, 1989: Cloud radiative forcing and climate: Results from the Earth Radiation Budget Experiment. *Science,* **243,** 57-63.

Simmons, A.J., D.M. Burridge, M. Jarraud, C. Girard, and W. Wergen, 1988: The ECMWF medium-range prediction models, Development of the numerical formulations and the impact of increased resolution. *Meteor. Atmos. Phys.,* **40,** 28-60.

Slingo, J.M., 1987: The development and verification of a cloud prediction scheme for the ECMWF model. *Quart. J. Roy. Meteor. Soc.,* **113,** 899-928.

Tiedtke, M., 1989: A comprehensive mass-flux scheme for cumulus parameterization in large-scale models. *Mon. Wea. Rev.,* **117,** 1779-1800.

Tiedtke, M., W.A. Heckley, and J. Slingo, 1988: Tropical forecasts at ECMWF: On the influence of physical parameterization on the mean structure of forecasts and analyses. *Quart. J. Roy. Meteor. Soc.*, **114,** 639-664.